Ultrafast Dynamics of Solute Molecules Probed by Resonant Optical Kerr Effect Spectroscopy

Soh Kushida,[*, †, ‡] *Kuidong Wang,*[†, //] *Cyriaque Genet,*[†] *Thomas W. Ebbesen*[†]

† University of Strasbourg, CNRS, ISIS & icFRC, 8 allée Gaspard Monge, 67000 Strasbourg, France

‡ Faculty of Pure and Applied Sciences, and Tsukuba Research Center for Energy Materials Science (TREMS) University of Tsukuba, 1-1-1 Tennodai, Japan

// Current address: Key Laboratory for Physical Electronics and Devices of the Ministry of Education & Shaanxi Key Lab of Information Photonic Technique, School of Electronics & Information Engineering, Xi'an Jiaotong University, Xi'an, 710049, China

AUTHOR INFORMATION

Corresponding Author

*Dr. Soh Kushida - University of Strasbourg, CNRS, ISIS & icFRC, 8 allée Gaspard Monge, 67000 Strasbourg, France

-Faculty of Pure and Applied Sciences, and Tsukuba Research Center for Energy Materials Science (TREMS) University of Tsukuba, 1-1-1 Tennodai, Japan

Email: kushida@unistra.fr

ABSTRACT: Ultrafast molecular dynamics in fluids is of great importance in many biological and chemical systems. Although such dynamics in bulk liquids has been explored by various methods, experimental tools that unveil the dynamics of solvated solutes are limited. In this work, we have developed resonant optical Kerr-effect spectroscopy (ROKE), which is an analog of optical Kerr-effect spectroscopy that measures the reorientational relaxation of a dilute solute in solution. By adjusting the pump and probe wavelengths at the resonant absorption band of a solute, the time response of the solute was distinguished easily from the negligible signal of the solvent. The heterodyne detection of ROKE enables the determination of reorientational relaxation time constants with an accuracy of 2.6%. The signal-to-noise ratio was high enough (average~26.7) to obtain an adequate signal from even a 10 μM solution. Thus, ROKE is a powerful tool to study solute dynamics with high sensitivity in a broad range of applications.

TOC GRAPHIC

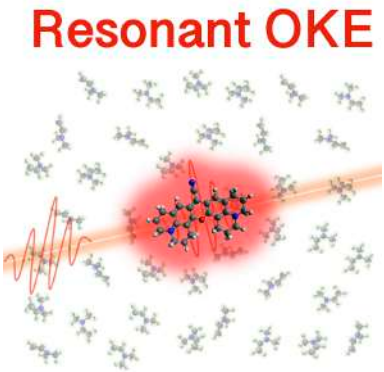

KEYWORDS pump-probe, solvation, reorientational relaxation, liquid-liquid phase separation

Solute-dynamics and intermolecular interactions between a solute and a solvent play important roles in molecular processes such as chemical reactions and biological phenomena.[1–4] In solution,

solvation affects the distribution and organization of solvent molecules around the solute, resulting in non-straightforward dynamics and corresponding reactions/phenomena.[5–7] Since the microscopic dynamics cannot be simply predicted from macroscopic properties such as the dielectric constant or viscosity, it is essential to investigate the processes at the molecular level to reveal the mechanisms of the dynamics that take place in heterogeneous media. For instance, it was just recently found that liquid-liquid phase separation plays a crucial role in many biological systems, gaining more attention.[8–13] Hence, experimental techniques that probe solutions at the molecular level are very important to explore elusive chemical/biological issues, but also challenging due to the sophisticated nature of liquids.

A variety of optical techniques have been developed in order to investigate various dynamics of fluids.[14–18] Among them, Optical-Kerr effect spectroscopy (OKE) is a powerful pump-probe technique that can measure the orientational dynamics of a transparent liquid by tracing the transient birefringence.[19–32] OKE measures convolution of polarizability tensor in a time domain, providing information about many events induced by electronic and nuclear responses including reorientational relaxation of bulk fluids.[19–24] Additionally, OKE can also determine the third-order nonlinear susceptibilities ($\chi^{(3)}$) since the signal intensity of OKE depends on $\chi^{(3)}$. Although the major topics of OKE studies are transparent liquids, OKE has also been applied to dye solutions or semiconductors.[25–34] Remarkably, these studies clarified that $\chi^{(3)}$ of a dye molecule is generally several orders of magnitude larger than that of the solvent, particularly at the resonant excitation wavelengths of the solute.[25–28,32] The effect facilitates the detection of a solute even in dilute conditions. For example, the time responses of photoinitiated solvation were studied by

polarizability response spectroscopy (PRS), an analog of OKE spectroscopy.[29–31] The resonant-pump/non-resonant probe system of PRS can track the dynamics simultaneously of both solute and solvent, providing information about the ultrafast solvation processes. However, OKE spectroscopy with resonant-pump/resonant-probe (ROKE) has never been studied as a tool for dynamics studies despite the fact that it allows one to collect a discrete signal from the solute and is therefore expected to have much higher sensitivity. Furthermore, reorientational relaxation of solutes has been less studied by OKE analogue techniques though the orientational relaxation process provides a lot of important information. [29–31,35]

In this work, we have developed an OKE technique with resonant-pump and resonant-probe, (ROKE), focusing on the solute reorientational relaxation dynamics (Figure 1a). Adjusting the pump-probe wavelength at a resonant band of a solute enables the detection of the distinct reorientational time response of the solute in solution, all the while the solvent signal remains negligible (Figure 1 b, c). The sensitivity and accuracy of this approach are excellent in comparison to other techniques that measure reorientational relaxation of a solute, suggesting that ROKE is a promising tool for potential applications such as studies of liquid-liquid phase separation.[11–13]

For ROKE measurements, we implemented an analogous setup to heterodyne-detected optical Kerr-effect spectroscopy (HD-OKE) but with both pump and probe beams at resonant wavelengths. [20–25,36] The detailed setup is shown in Figure S1. The key components shall be described below.

In our ROKE setup, the 800 nm ultrashort pulse was generated from a Ti:sapphire laser system, which consists of an 80 MHz oscillator and a 1000 Hz amplifier. The center wavelength, the pulse width, and the repetition rate of the laser system are 800 nm, 100 fs, and 1000 Hz, respectively. The optional resonant wavelength was obtained from an optical parametric amplifier. The output

light was split into pump and probe parts. The pump light arrives at the sample with horizontal polarization, and the probe beam is polarized at 45º relative to the pump beam through a half-wave plate and a polarizer (P1). Between a sample and P1, a quarter-wave plate (QWP) is placed with its fast axis at 45º. Both P1 and QWP are mounted on motorized rotation stages for precise angular control. After the probe beam reaches the sample, the beam is filtered by another polarizer (P2) at -45º to detect a birefringent signal. Modulation of the time delay between pump and probe beams gives time-dependent responses. The pump and probe beams are focused and attenuated to obtain 127 μJ/cm^2 and 40 μJ/cm^2 with spot sizes of 200 μm and 500 μm in diameter, respectively. The calibration must be performed for each sample to compensate for the slight birefringence induced by experimental elements such as the cuvette (see Calibration in Supporting Information). The measurements are typically performed with P1 angles at 45± αº (α is a small angle, typically 2) for a sample and a differential signal of the two signals (a heterodyne signal) is constructed arithmetically. At least 3 scans are swept along time delay for each measurement. A signal-to-noise ratio is defined as an averaged signal divided by the standard deviation.

The simplest OKE measurement is so called homodyne detection, in which the angle of P1 is at 45º. In this condition, QWP does not play any role because the fast axis is parallel to P1. The homodyne signal intensity (I_{homo}) and the homodyne signal field (E_{homo}) can be described as[36]

$$\sqrt{I_{homo}} = E_{homo} = i\ \chi_{eff}^{(3)}\, I_{pump}\, E_{probe} \qquad (1)$$

where I_{pump}, E_{probe}, and $\chi_{eff}^{(3)}$ denote the pump laser intensity, the probe laser field, and the effective third-order nonlinear susceptibility, respectively. Since the observable in the experiment is I_{homo}, the signal decays as it's square root (Eq. 1) and the quality of the signal-to-noise ratio as

well as deviations at long-times would be poor. Hence, we employed a heterodyne-detection technique. In the heterodyne technique, P1 is slightly (a few degrees, α) tilted to have small leakage that is orthogonal to the major component of the probe beam. The leakage becomes 90º out of the phase due to the QWP that follows in the setup (Fig. 1), and the leakage acts as a local oscillator that is mixed with the homodyne signal in phase. The out of phase ($E_{l.o.}$) field of the local oscillator can be expressed as [36]

$$E_{l.o.} = i\alpha E_{probe} \tag{2}$$

assuming that sin αº ~ α (rad). The local oscillator interferes with the signal and, as a consequence, the total signal ($I_{total,\alpha}$) and field ($E_{total,\alpha}$) are given by

$$\begin{aligned} I_{total,\alpha} &= \left|E_{total,\alpha}\right|^2 = (E_{homo} + E_{l.o.})(E_{homo}^* + E_{l.o.}^*) \\ &= I_{homo} + I_{l.o.} + Re[E_{homo}^* E_{l.o.} + E_{homo} E_{l.o.}^*] \end{aligned} \tag{3}$$

where $I_{l.o.}$ is the intensity of the local oscillator, which is expressed as

$$I_{l.o.} = \alpha^2 I_{probe} \tag{4}$$

We note that a lock-in amplifier chops out $I_{l.o.}$ for the cases of conventional OKEs. However, $I_{l.o.}$ remains a finite value in the heterodyne signal of ROKE because the pump pulse induces excitations and the corresponding transient absorption/bleaching. Eq. (1)-(4) lead to

$$I_{total,\alpha} = I_{homo} + \alpha^2 I_{probe} - 2\alpha\, Re\left[\chi_{eff}^{(3)}\right] I_{pump} I_{probe} \tag{5}$$

Here, only the third term is an odd function of α, while the first and second terms are even functions. This enables the arithmetical construction of a heterodyne signal ($I_{hetero,|\alpha|}$) by subtracting a total signal at one angle ($I_{\mathrm{total},\alpha}$) from a total signal at the opposite angle($I_{\mathrm{total},-\alpha}$) as

$$I_{hetero,|\alpha|} = I_{total,-\alpha} - I_{total,\alpha} = 4\alpha\, Re\left[\chi^{(3)}_{eff}\right] I_{pump}\, I_{probe} \tag{6}$$

To be valid, Eq. (6) implies that ±α must be strictly calibrated, and therefore P1 and QWP. As shown in Eq. (6), the heterodyne signal is proportional to the real part of the $\chi^{(3)}_{eff}$,$Re\left[\chi^{(3)}_{eff}\right]$, contrary to homodyne signal in Eq. (1). This facilitates a high signal-to-noise ratio, especially in the long-time range. The nonlinear optical response (R(t)) is proportional to $\chi^{(3)}_{eff}$, itself a function of the time delay between pump and probe. R(t) is considered to be a combination of several parameters such as electronic hyperpolarizability, low-frequency vibrations, and reorientational relaxations. Among them, reorientational relaxation is a relatively slow-decay component and dominates the signal after a picosecond. Since we only highlight the reorientational relaxation after a picosecond in this work, other components won't be discussed. The orientational relaxation time (τ_{rot}) is typically a mono-exponential decay.[36] R(t) is, therefore, approximated as a linear combination of singular components in accordance with the singular value decomposition:[35,37]

$$R\,(t) = \sum_{i=ex,g,and\ solvent} I_i\, Exp(-t/\tau_{i,rot}) \tag{7}$$

Where $I_i = D_i\, W_i$ with D_i and W_i that indicate the density of molecules *i* and the weighting constant of the non-linear response of *i*, respectively. We clearly discriminate between excited solute molecules (ex) and ground state ones (g) because W_{ex} is typically much larger than W_g or

$W_{solvent}$ as we will also justify in the following paragraph. With the density of solute (D_{solute}) and the lifetime of the excited state (τ_{ex}), I_{ex} and I_g can be expressed by

$$I_{ex} = W_{ex}D_{ex} = W_{ex}D_{solute}Exp(-t/\tau_{ex}),$$
$$I_g = W_gD_g = W_gD_{solute}\{1 - Exp(-t/\tau_{ex})\} \quad (8)$$

respectively. Here, I_{ex} corresponds to the transient dynamics of the refractive index (Δn_{ex}) induced by a resonant pump. At resonant wavelength, I_g and $I_{solvent}$ are negligible and the signal of solute can dominate R(t), provided an adequate concentration (D_{solute} / $D_{solvent}$) and a sufficiently long τ_{ex}. Accordingly, Eq. (7) at resonant wavelength is transformed to

$$Re\left[\chi^{(3)}_{eff}\right](t) \propto R(t) \approx \Delta n_{ex}Exp\left(-t/\tau_{rot,solute}\right)$$
$$= W_{ex}D_{solute}Exp\left(-t/\tau_{ex} - t/\tau_{rot,solute}\right) \quad (9)$$

We note that I_{probe} in Eq. (6) is a constant. In addition, the excited transient absorption (ΔA) caused by the pump fluence induces only a negligible absorption deviation ($\Delta A/A$ ~10^{-4}, Figure S2). Therefore, the heterodyne signal in Eq. (6) can be fitted with the mono-exponential model as in Eq. (9).

Rhodamine 800 and N, N-dimethylformamide (DMF) were employed as a solute and a solvent in our experiments, respectively. An absorption peak at 691 nm is clearly observed in the absorption spectrum of 50 μM R800 solution in DMF (Figure 2a). We performed angle-dependent ROKE measurements with the pump and probe beams at the absorption peak of R800. The corresponding time-resolved signals are shown in Figure 2b. The shapes and signs of the signals vary depending on α, indicating that the signals are composed of multiple dynamic processes. The signal at α = 0º (I_0) is considered I_{homo}. In order to understand the components involved in the signals at various

angles (I_{x° for the angle x^o), I_0 was subtracted from each signal (I_{x° - I_0) since I_{homo} is supposed to be involved in all the cases. Figure 2c is an example for I_{-2° - I_0. According to Eq. (5), one can expect two components, that are proportional to α^2 and α, respectively. The former is associated with the leakage (intensity of local oscillator, $I_{l.o.}$) that decays with the lifetime of the excited state (τ_{ex}) which for R800 was determined 1.02 ns by performing degenerated pump-probe experiments and transient absorption measurements without polarizers (Figure S2 and TableS1). The latter is the heterodyne signal as described in Eq. (9). Both components are supposed to decay mono-exponentially. Therefore, we performed a biexponential fitting of I_{-2° - I_0 with the fixed value of τ_{ex}, 1.02 ns. The fitting can be found as a purple curve in Figure 2c. The differential signals of other angles were also fitted with the same model (Figure S3). The weight components, I_{hetero} and $I_{l.o.}$, were extracted and plotted as a function of α (Figure 2d and Table S2). $I_{l.o.}$ and I_{hetero} were fitted with $I_{l.o.}$=0.0037α^2 and I_{hetero} = 0.09α, respectively as expected in Eq. (5) (dot lines in Figure 2d). Indeed, signals obtained from conventional OKEs (non-resonant OKE) do not contain $I_{l.o.}$, so that any differential signal of two angles should be mono-exponential regardless of the choice of two. Therefore, the biexponential shapes of the differential signals of ROKE and the resulting fittings verify our assumption in Eq. (5). It is worth noting that the α-dependent heterodyne component is slightly away from a linear shape. This is because Eq. (2) stands on the basis that sin $\alpha^o \sim \alpha$ (rad). When α becomes larger, the approximation is no longer valid. It is rather natural that the slope becomes sigmoidal at a large angle. In order to obtain parameters concerning reorientational relaxation, we canceled out I_{homo} and $I_{l.o.}$ by differentiating the obtained signals at ± α. Figure 2e shows a processed signal, I_{-2° - I_{+2°. The signal on a logarithmic y-scale is linear with respect to the time delay, suggesting a mono-exponential decay characteristic. In addition, I_{-1° - I_{+1° and I_{-3° - I_{+3° also demonstrate mono-

exponential decays with comparable time constants as that of I_{-2° - I_{+2° (Figure S4 and Table S3). Signal-to-noise ratios are high enough (average: ~20) in the whole-time range (Figure S4d-e). The obtained time constant of heterodyne signal (τ_{hetero}) can be decomposed into a reorientational decay time (τ_{rot}) and an excited state lifetime (τ_{ex}) as indicated in Eq. (9). τ_{rot} of R800 solution was determined 102.9 ±2.42 ps. This value is distinct from that of pure DMF solvent (3,65 ps, Figure 2f). Additionally, the heterodyne signal intensity of the pure DMF is one order of magnitude weaker than that for the 50 µM R800 solution. These facts confirm that the response of R800 is dominant in the heterodyne signal of the solution. We would like to emphasize that the fitting residuals shown in Figure 2e are very small (average ~7%), indicating the surprisingly small deviation of the measured signal. The residuals here are normalized by the signal intensity (see details in the experimental section in SI). Thereby, a high coefficient of determination (R^2: ~0.999) is obtained.

In order to gain more insights into ROKE, concentration-dependent and wavelength-dependent measurements were carried out. As shown in Figure 3a, the signal intensity of R800 solution increases with respect to the concentration while the decay time remains essentially unchanged (107.49 ±8.0 ps). The fittings and the resulting parameters are given in Figure S5 and Table S4. We would like to mention that the signal intensity at the concentration of 200 µM drops drastically. This is possibly assigned to the low transmittance of a probe beam (2%). The sensitivity of ROKE is exceptionally high; $\tau_{rot,solute}$ was determined with R^2 of 0.996 even for a 10 µM solution in a 1 mm cuvette. Signal-to-noise ratios are reliable enough (~20) for all concentrations obtained from 3 scans (Figure S6, Table S4). The signal of the solute at 10 µM is still 7.5 times larger than that of the solvent. The absolute intensity of the signal can be amplified by simply increasing the pump fluence or by using a thicker cuvette. Hence, we believe that $\tau_{rot,solute}$ in an even lower

concentration sample can be detected, provided a photo-stable solute. Simultaneously, we also believe that a more concentrated sample can be also measured by using a thinner cuvette such as several micrometer thick IR cells. We would also like to mention that the heterodyne signals for 10 μM and 20 μM solutions deviate from the fittings in a long-time range. We attribute this to the appearance of incomplete compensation of $I_{l.o.}$ due to the relatively weak heterodyne signals in the long-time range. This assumption is reasonable because the fitting in Figure S5a'-b'are consistent with the experimental results when a small but nonnegligible fraction of $I_{l.o.}$ is considered.

ROKE signals at various wavelengths are shown in Figure S7. At the wavelength that is far from the resonant band of R800, the resonant effect of $\chi^{(3)}$ must be weak. The approximation in Eq. (9) transformed from Eq. (7) is not valid at the non-resonant wavelength. The contribution from DMF cannot be neglected at some wavelengths and thus two components in heterodyne signals from both DMF and R800 (I_{DMF} and I_{R800}, respectively) should be considered. We performed singular value decomposition utilizing Eq. (S3) with the fixed decay time obtained from the above experiments, obtaining the weighting components (Figure S7). The best-fitted parameters for I_{DMF} and I_{R800} are shown in Table S5 and plotted in Figure 3b. While I_{DMF} remains nearly intact, I_{R800} varies over 2 orders of magnitudes with the maximum value at the resonant condition. Such large contrast near the resonant band indicates that I_{DMF} can be neglected at the resonant wavelength of R800. We note that we can yet distinguish the two signals at the slightly detuned wavelengths for this specific solution because the time constants of R800 and DMF are an order of magnitude different. However, the usage of resonant wavelength in non-linear spectroscopy proffers a universal methodology to detect solute dynamics regardless of the contribution from a solvent. Interestingly, the sign of I_{R800} is inverted above 691 nm. We assigned this to the sign of

Δn_{ex}, taking Eq. (9) into account. The dotted line in Figure3b denotes Δn_{ex} of R800 obtained by the Kramers-Kronig transformation of a transient absorption spectrum (Figure S2).[38] It is apparent that the signs of I_{R800} comply with those of Δn_{ex}. For the case at the fully non-resonant wavelength (770 nm), the signal of R800 could not be found. We also performed OKE experiments with non-resonant pump/resonant probe (FigureS8). Though the relative intensity of R800 (I_{R800} / I_{DMF}) at this condition is smaller than that for resonant pump/ resonant probe, the reorientational decay of R800 on the ground state could be clearly seen with the comparable $\tau_{rot,solute}$. It is in clear contrast to the non-resonant pump/ non-resonant probe system, indicating that employing resonant wavelengths for both pump and probe can amplify the signal of a dye. The comparisons can be also found in Table S6

Generally, a solute in solution is solvated by solvent molecules and isolated from other solute molecules. Therefore, ROKE is expected rather sensitive to the microscopic environment around a solute molecule. We further examined ROKE measurements of R800 in 8 different solvents. In addition to DMF, acetone, benzonitrile (BN), tetrahydrofuran (THF), water, heavy water, propylene carbonate (PC), and isopopanol (IPA) were examined. They are all capable of dissolving R800 and many parameters of them including viscosity are different (Table S7). We prepared 3 identical solutions independently for each solvent. Obviously, the time constant for the reorientational relaxation of R800 is dependent on solvents (Figure 4a, Figure S9). Historically, reorientational relaxation of solutes has been well studied by the means of anisotropic transient absorption spectroscopy (ATAS) and time-resolved fluorescence anisotropy (TRFA). [39–45] It is well known that reorientational relaxation is governed by the Stokes-Einstein-Debye (SED) relation,[46] which is

$$\tau_{rot} = \frac{V\eta}{k_B T} \tag{10}$$

where V, η, k_B, T are a molecular volume, the shear viscosity, the Boltzmann constant, and the temperature, respectively. The time constants for each solvent, which are averaged over 3 independent solutions, are shown in Figure 4b. τ_{rot} increases nearly linearly with respect to η. However, the slope is not found to be 1, but 0.78 when carefully compared on a logarithmic scale (inset of Figure 4b). Indeed, previous TRFA studies clarified the relaxation time of some dyes could be expressed as $\tau_{rot} \propto \eta^x$ ($x \leq 1$).[39,42,43] Therefore, the results possibly indicate the breakdown of the simple SED law for R800. ROKE is advantageous for in-depth studies of the solute-dynamics in a solution system owing to the excellent signal resolution. The heterodyne-detection of ROKE enables a high signal-to-noise ratio (~20), high signal resolution over 3 orders of magnitudes with a small signal deviation (~7% to the signal), and obtaining reliable time constants with an extremely small deviation (2.6% on average). By comparison, TRFA and ATAS as schemes built on polarized intensity ratios, whose signal resolution is intrinsically limited to an order of magnitude due to relatively large signal fluctuations (typically ~40% to the signal).[44,45] Therefore, measuring reorientational dynamics using ROKE instead of TRFA or ATAS might lead to new insights whenever highly sensitive measurements are required. Besides, ROKE relies on absorption and nonlinearity, broadening the available window of the solute molecules (e.g. non-fluorescent molecules). As pointed out in the introduction, the dynamics of complex fluids have recently been recognized as essential in a biological system.[7–9] ROKE is potentially useful for such studies, provided appropriate dyes that can be dissolved selectively in a specific phase are used.

In conclusion, we have established resonant Kerr-effect spectroscopy (ROKE) that tracks reorientational relaxation of a solute molecule in solution. The key factors are resonant pump-probe beams, which rule out unwanted signals owing to the high nonlinearity of a solute at a resonant wavelength. As a result, a sufficient signal over 3 orders of magnitudes was obtained even from a 10 μM solution with an extremely small deviation. Since the heterodyne detection can determine relaxation time quite accurately (~± 2.6%), we demonstrated a linear correlation between the reorientational relaxation time and the viscosity governed by the modified SED law. We expect ROKE to be a powerful tool for gaining insights into the microscopic environment around solute molecules, providing an alternative approach in the fields of biology, material science, and physical chemistry.

FIGURES

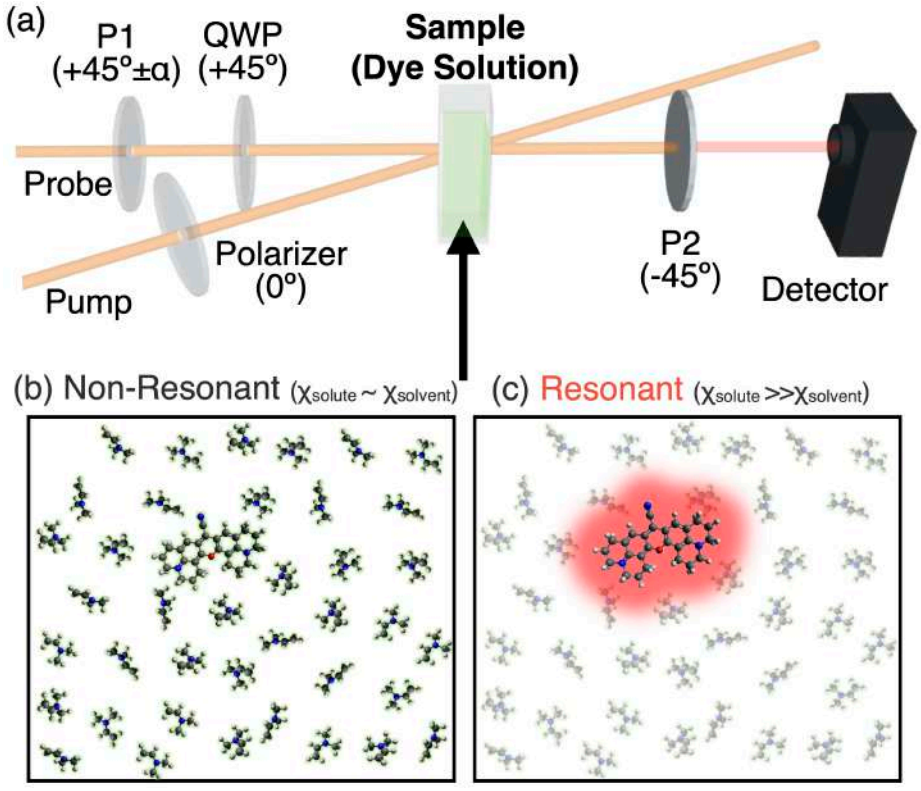

Figure 1. (a) A schematic illustration of resonant Kerr-effect spectroscopy. Microscopic illustrations in a solution sample under pump-probe beams at non-resonant wavelength (b) and resonant wavelength (c).

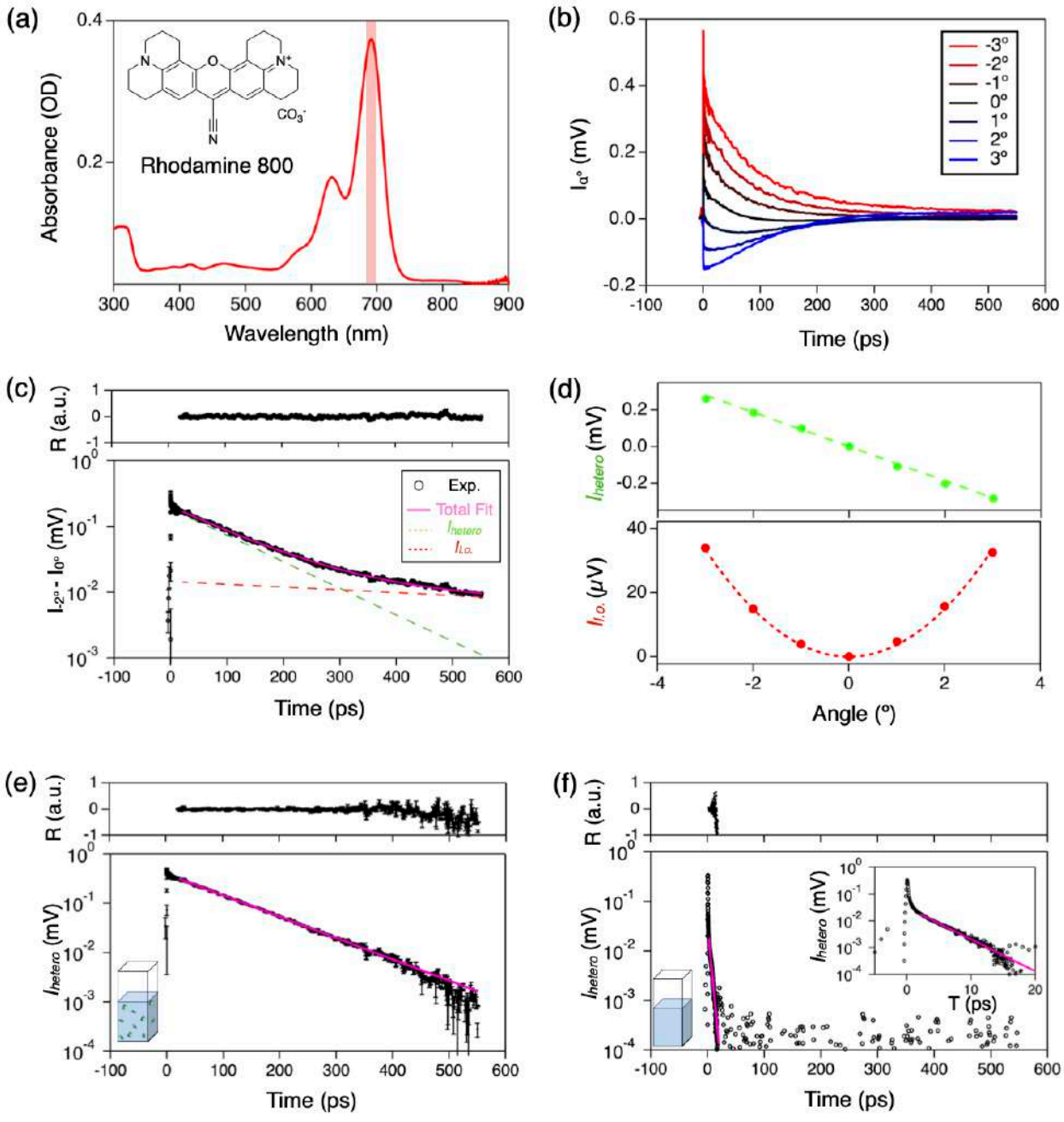

Figure 2. (a) Absorption spectra of R800 dissolved in DMF. The inset shows a chemical structure of R800. (b) Unprocessed signals of ROKE measurements of R800 solution with respect to angle α. (c) A differential signal of ROKE signals at α =-2° and α = 0° (I_{-2° - I_0). The purple line indicates a fitted curve with the double exponential model (Eq.(5)). The green and red dot lines are decomposed decays of a heterodyne signal (I_{hetero}) and leakage ($I_{l.o.}$), respectively. (d) The best-fitted compositions of I_{hetero} and $I_{l.o.}$ as a function of α. Dot lines are linear (green) and square root (red) fittings, respectively. Heterodyne signals (black) of R800 solution (e) and pure DMF (f). The purple lines show fitted curves with the mono-exponential model. The inset in (f) shows the identical signal in a short time range. The top graphs in (c, e, f) indicate residuals of the fittings.

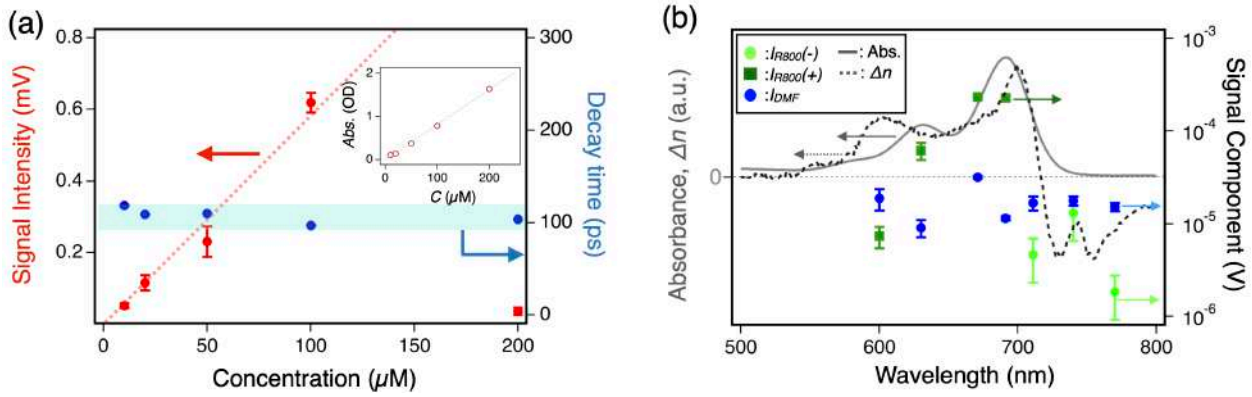

Figure 3. (a) ROKE signal intensity (red) and decay time as a function of the concentration of R800 in DMF. The inset shows absorbance at 691 nm *versus* a concentration of R800. (b) Decomposed coefficients for R800 (green) and DMF (blue) as a function of wavelength. The light green and dark green show negative and positive values, respectively. The gray line and the dotted line show the ground state absorption spectrum and a transient refractive index spectrum (at 50 ps) of R800 solution, respectively.

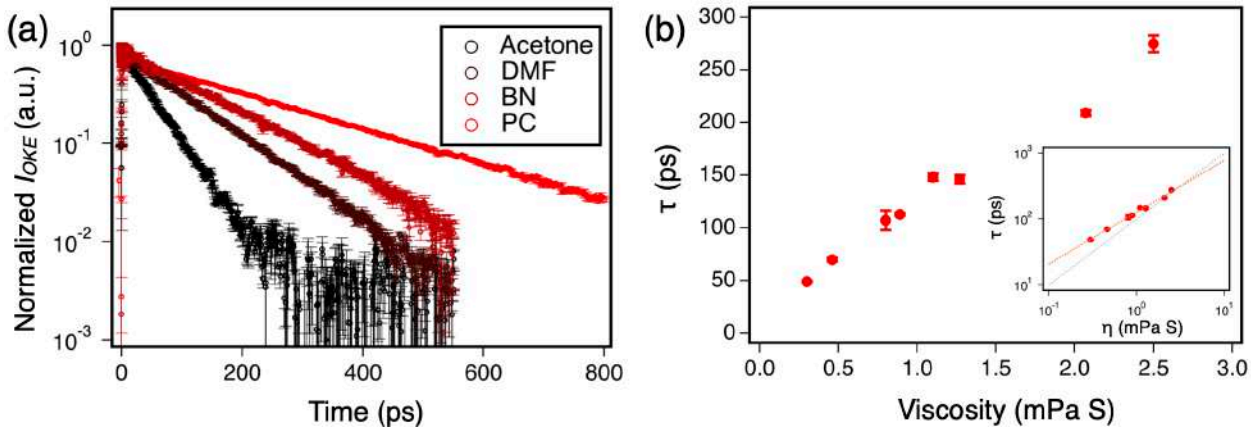

Figure 4. (a) ROKE signals of R800 in Acetone, DMF, BN, and PC (black to red). (b) The averaged reorientational relaxation time as a function of solvent viscosity. The error bar shows the standard deviation extracted from 3 independent measurements. The inset shows the identical data on a logarithmic scale. The black and red lines indicate slopes of 1 and 0.77, respectively.

ASSOCIATED CONTENT

Supporting Information.

The following files are available free of charge.

General information, experimental section, supporting figures (a schematic illustration of the setup, transient absorption spectra of R800, fitting results of experimental data, signal-to-noise ratios), tables (fitting parameters), and supporting reference are available(PDF)

AUTHOR INFORMATION

Notes

The authors declare no competing financial interests.

ACKNOWLEDGMENT

S.K. is grateful to JSPS KAKENHI (Grant Number JP20J00845) for the financial support. T.W.E. acknowledges the funding support of the ERC (project no. 788482 MOLUSC) and USIAS within

the Investissement d'Avenir program ANR-10-IDEX-0002-02. We also acknowledge support from the International Center for Frontier Research in Chemistry (icFRC, Strasbourg),

REFERENCES

(1) Reichardt, C. *Solvents and Solvent Effects in Organic Chemistry*; VCH: New York, 1990.

(2) Alberts, B.; Johnson, A.; Lewis, J.; Raff, M.; Roberts, K.; Walter, P. *Molecular Biology of the Cell, Garland Science*; Garland Science: New York, 2002.

(3) Karplus, M.; Petsko, G. A. Molecular Dynamics Simulations in Biology. *Nature* **1990**, *347*, 631–639.

(4) Rossky, P. J.; Simon, J. D. Dynamics of Chemical Processes in Polar Solvents. *Nature* **1994**, *370*, 263–269.

(5) Rosspeintner, A.; Lang, B.; Vauthey, E. Ultrafast Photochemistry in Liquids. *Annu. Rev. Phys. Chem.* **2013**, *64*, 247–271.

(6) Cramer, C. J.; Truhlar, D. G. A Universal Approach to Solvation Modeling. *Acc. Chem. Res.* **2008**, *41*, 760–768.

(7) Dopfer, O.; Fujii, M. Probing Solvation Dynamics around Aromatic and Biological Molecules at the Single-Molecular Level. *Chem. Rev.* **2016**, *116*, 5432–5463.

(8) Brangwynne, C. P.; Eckmann, C. R.; Courson, D. S.; Rybarska, A.; Hoege, C.; Gharakhani, J.; Jülicher, F.; Hyman, A. A. Germline P Granules Are Liquid Droplets That Localize by Controlled Dissolution/Condensation. *Science* **2009**, *324*, 1729–1732.

(9) Shiraki, K.; Mimura, M.; Nishinami, S.; Ura, T. Effect of Additives on Liquid Droplets and Aggregates of Proteins. *Biophys. Rev.* **2020**, *12*, 587–592.

(10) Kushida, S.; Oki, O.; Saito, H.; Kuwabara, J.; Kanbara, T.; Tashiro, M.; Katouda, M.; Imamura, Y.; Yamamoto, Y. From Linear to Foldamer and Assembly: Hierarchical Transformation of a Coplanar Conjugated Polymer into a Microsphere. *J. Phys. Chem. Lett.* **2017**, *8*, 4580–4586.

(11) Leys, J.; Losada-Ṕrez, P.; Cordoyiannis, G.; Cerdeiriña, C. A.; Glorieux, C.; Thoen, J. Temperature, Concentration, and Frequency Dependence of the Dielectric Constant near the Critical Point of the Binary Liquid Mixture Nitrobenzene-Tetradecane. *J. Chem. Phys.* **2010**, *132,* 04508.

(12) Simeoni, G. G.; Bryk, T.; Gorelli, F. A.; Krisch, M.; Ruocco, G.; Santoro, M.; Scopigno, T. The Widom Line as the Crossover between Liquid-like and Gas-like Behaviour in Supercritical Fluids. *Nat. Phys.* **2010**, *6,* 503–507.

(13) Toyouchi, S.; Kajimoto, S.; Barzan, D.; Kiel, A.; Enderlein, J.; Fukumura, H.; Herten, D. P. Observation of Unusual Molecular Diffusion Behaviour below the Lower Critical Solution

Temperature of Water/2-Butoxyethanol Mixtures by Using Fluorescence Correlation Spectroscopy. *ChemPhysChem* **2014**, *15*, 3832–3838.

(14) Tielrooij, K. J.; Paparo, D.; Piatkowski, L.; Bakker, H. J.; Bonn, M. Dielectric Relaxation Dynamics of Water in Model Membranes Probed by Terahertz Spectroscopy. *Biophys. J.* **2009**, *97*, 2484–2492.

(15) Arnolds, H.; Bonn, M. Ultrafast Surface Vibrational Dynamics. *Surf. Sci. Rep.* **2010**, *65*, 45–66.

(16) Perakis, F.; de Marco, L.; Shalit, A.; Tang, F.; Kann, Z. R.; Kühne, T. D.; Torre, R.; Bonn, M.; Nagata, Y. Vibrational Spectroscopy and Dynamics of Water. *Chem. Rev.* **2016**, *116*, 7590–7607.

(17) Damari, R.; Kallush, S.; Fleischer, S. Rotational Control of Asymmetric Molecules: Dipole-versus Polarizability-Driven Rotational Dynamics. *Phys. Rev. Lett.* **2016**, *117*, 103001.

(18) Damari, R.; Rosenberg, D.; Fleischer, S. Coherent Radiative Decay of Molecular Rotations: A Comparative Study of Terahertz-Oriented versus Optically Aligned Molecular Ensembles. *Phys. Rev. Lett.* **2017**, *119*, 033002.

(19) Palese, S.; Schilling, L.; Miller, R. J. D.; Staver, P. R.; Lotshaw, W. T. Femtosecond Optical Kerr Effect Studies of Water. *J. Phys. Chem.* **1994**, *98*, 6308–6316.

(20) Turton, D. A.; Wynne, K. Universal Nonexponential Relaxation: Complex Dynamics in Simple Liquids. *J. Chem. Phys.* **2009**, *131,* 201101.

(21) Zhong, Q.; Fourkas, J. T. Optical Kerr Effect Spectroscopy of Simple Liquids. *J. Phys. Chem. B.* **2008**, *112*, 15529–15539.

(22) Torre, R.; Bartolini, P.; Righini, R. Structural Relaxation in Supercooled Water by Time-Resolved Spectroscopy. *Nature* **2004**, *428*, 296–299.

(23) Hunt, N. T.; Jaye, A. A.; Meech, S. R. Ultrafast Dynamics in Complex Fluids Observed through the Ultrafast Optically-Heterodyne-Detected Optical-Kerr-Effect (OHD-OKE). *Phys. Chem. Chem. Phys.* **2007**, *9*, 2167–2180.

(24) Yamada, S. A.; Bailey, H. E.; Fayer, M. D. Orientational Pair Correlations in a Dipolar Molecular Liquid: Time-Resolved Resonant and Nonresonant Pump-Probe Spectroscopies. *J. Phys. Chem. B.* **2018**, *122*, 12147–12153.

(25) Slepkov, A. D.; Hegmann, F. A.; Zhao, Y.; Tykwinski, R. R.; Kamada, K. Ultrafast Optical Kerr Effect Measurements of Third-Order Nonlinearities in Cross-Conjugated Iso-Polydiacetylene Oligomers. *J. Chem. Phys.* **2002**, *116*, 3834–3840.

(26) Petruska, M. A.; Malko, A. v.; Voyles, P. M.; Klimov, V. I. High-Performance, Quantum Dot Nanocomposites for Nonlinear Optical and Optical Gain Applications. *Adv. Mater.* **2003**, *15*, 610–613.

(27) Liu, Y.; Zhang, C.; Wang, R.; Zhang, B.; Tan, Z.; Wang, X.; Xiao, M. Large Optical Nonlinearity Induced by Singlet Fission in Pentacene Films. *Angew. Chem. Int. Ed.* **2015**, *54*, 6222–6226.

(28) Ohara, K.; Yamada, T.; Tahara, H.; Aharen, T.; Hirori, H.; Suzuura, H.; Kanemitsu, Y. Excitonic Enhancement of Optical Nonlinearities in Perovskite CH3NH3PbCl3 Single Crystals. *Phys. Rev. Mater.* **2019**, *3,* 111601.

(29) Underwood, D. F.; Blank, D. A. Ultrafast Solvation Dynamics: A View from the Solvent's Perspective Using a Novel Resonant-Pump, Nonresonant-Probe Technique. *J. Phys. Chem. A* **2003**, *107*, 956–961.

(30) Park, S.; Flanders, B. N.; Shang, X.; Westervelt, R. A.; Kim, J.; Scherer, N. F. Solvent Intermolecular Polarizability Response in Solvation. *J. Chem. Phys.* **2003**, *118*, 3917–3920.

(31) Park, S.; Kim, J.; Moran, A. M.; Scherer, N. F. Solvent Structural Relaxation Dynamics in Dipolar Solvation Studied by Resonant Pump Polarizability Response Spectroscopy. *Phys. Chem. Chem. Phys.* **2011**, *13*, 214–223.

(32) Vigil, S. R.; Kuzyk, M. G. Absolute Molecular Optical Kerr Effect Spectroscopy of Dilute Organic Solutions and Neat Organic Liquids. *J. Opt. Soc. Am. B* **2001**, *18*, 679-691.

(33) Zhu, H.; Miyata, K.; Fu, Y.; Wang, J.; Joshi, P. P.; Niesner, D.; Williams, K. W.; Jin, S.; Zhu, X.-Y. Screening in Crystalline Liquids Protects Energetic Carriers in Hybrid Perovskites. *Science* **2016**, *353*, 1409–1413.

(34) Miyata, K.; Meggiolaro, D.; Trinh, M. T.; Joshi, P. P.; Mosconi, E.; Jones, S. C.; de Angelis, F.; Zhu, X.-Y. Large Polarons in Lead Halide Perovskites. *Sci. Adv.* **2017**, *3*, 1701217.

(35) Ki, H.; Choi, S.; Kim, J.; Choi, E. H.; Lee, S.; Lee, Y.; Yoon, K.; Ahn, C. W.; Ahn, D. S.; Lee, J. H.; Park, J.; Eom, I.; Kim, M.; Chun, S. H.; Kim, J.; Ihee, H.; Kim, J. Optical Kerr Effect of Liquid Acetonitrile Probed by Femtosecond Time-Resolved X-Ray Liquidography. *J. Am. Chem. Soc.* **2021**, *143*, 14261–14273.

(36) Palese, S.; Schilling, L.; Miller, R. J. D.; Staver, P. R.; Lotshaw, W. T. Femtosecond Optical Kerr Effect Studies of Water. *J. Phys. Chem.* **1994,** *98*, 6308–6316.

(37) Kano, H.; Kobayashi, T. Time-Resolved Fluorescence and Absorption Spectroscopies of Porphyrin J-Aggregates. *J. Chem. Phys.* **2002**, *116*, 184–195.

(38) Lucarini, V.; Saarinen, J. J.; Peiponen, K.-E.; Vartiainen, E. M. Kramers-Kronig Relations in Optical Materials Research. *Springer Series in Optical Scicences* **2005**, *110*.

(39) Horng, M.-L.; Gardecki, J. A.; Maroncelli, M. Rotational Dynamics of Coumarin 153: Time-Dependent Friction, Dielectric Friction, and Other Nonhydrodynamic Effects. *J. Phys. Chem. A* **1997**, *101*, 1030–1047.

(40) Horng, M. L.; Gardecki, J. A.; Papazyan, A.; Maroncelli, M. Subpicosecond Measurements of Polar Solvation Dynamics: Coumarin 153 Revisited. *J. Phys. Chem.* **1995**, *99*, 17311–17337.

(41) Stratt, R. M.; Maroncelli, M. Nonreactive Dynamics in Solution: The Emerging Molecular View of Solvation Dynamics and Vibrational Relaxation. *J. Phys. Chem.* **1996**, *100*, 12981–12996.

(42) Williams, A. M.; Jiang, Y.; Ben-Amotz, D. Molecular Reorientation Dynamics and Microscopic Friction in Liquids. *Chem. Phys.* **1994**, *180*, 119–129.

(43) Spears, K. G.; Steinmetz, K. M. Solvent Interactions with Anions by Reorientation Studies of Resorufin. *J. Phys. Chem.* **1985**, *89*, 3623–3629.

(44) Chosrowjan, H.; Taniguchi, S.; Tanaka, F. Ultrafast Fluorescence Upconversion Technique and Its Applications to Proteins. *FEBS J.* **2015**, *282*, 3003–3015.

(45) Nguyen, H. K.; Konomi, A.; Sugimoto, S.; Inutsuka, M.; Kawaguchi, D.; Tanaka, K. Rotational Dynamics of a Probe in Rubbery Polymers Characterized by Time-Resolved Fluorescence Anisotropy Measurement. *Macromol. Chem. Phys.* **2018**, *219*, 1700329.

(46) Debye, P. *Polar Molecules*; Polar Molecules: New York, 1929.